Available online at www.sciencedirect.com
ScienceDirect
Trans. Nonferrous Met. Soc. China 31(2021) 24−35
Transactions of Nonferrous Metals Society of China
www.tnmsc.cn

# Quench sensitivity and microstructures of high-Zn-content Al−Zn−Mg−Cu alloys with different Cu contents and Sc addition

Ying-hao PENG, Chong-yu LIU, Li-li WEI, Hong-jie JIANG, Zhen-jiang GE

Key Laboratory of New Processing Technology for Nonferrous Metal & Materials, Ministry of Education, Guilin University of Technology, Guilin 541004, China

Received 20 March 2020; accepted 25 September 2020

**Abstract:** The Zn, Cu, and Sc contents of 7xxx Al alloys were adjusted according to the chemical composition of a 7085 Al alloy, and the effects of Zn and Cu contents and Sc addition on the microstructures, hardness, and quench sensitivity of the 7xxx Al alloys were studied. The alloys with high Zn content and Sc addition exhibited higher hardness than the 7085 alloy at the position 3 mm away from the quenching end. The density of $\eta$ and $T$ phases increased with the increase in Zn and Cu contents, and the Sc addition led to the formation of the $Y$ phase and more $\eta$ phases at the position 120 mm away from the quenching end. Compared with the 7085 alloy, the high Zn−high Cu and Sc-added alloys exhibited higher quench sensitivity, while the simultaneous increase in Zn content and decrease in Cu content could enhance the hardness and reduce the quench sensitivity of the 7085 alloy.

**Key words:** Al−Zn−Mg−Cu alloy; quench sensitivity; $Al_3(Sc,Zr)$; $Y$ phase; grain boundary

## 1 Introduction

Ultra-thick 7xxx (Al−Zn−Mg−Cu) alloy plates have been used in fabricating large components without welding [1,2]. Quench sensitivity and mechanical properties are the key indices for the application of ultra-thick Al alloys [3−5]. Thus, the improvement of quench sensitivity and mechanical properties of 7xxx Al alloys is becoming a priority in the aerospace industry.

The quench sensitivity and mechanical properties of 7xxx Al alloys mainly depend on the alloys' chemical compositions. Mg and Zn are the main strengthening elements of 7xxx Al alloys. ZHANG et al [6] and NIE et al [7] compared the quench sensitivity of several 7xxx Al alloys and found that the 7xxx Al alloys with low Mg content, such as 7085 alloys, have lower quench sensitivity. DENG et al [8] found that 0.6 wt.% Mg addition can decrease the quenching layer depth of a 7085 Al alloy from 70 to 40 mm and significantly increase quench sensitivity. In our previous study [9], additional Zn was added into a 7085 Al alloy. The increase in Zn content significantly reinforced the 7085 Al alloy and also slightly enhanced its quench sensitivity. Thus, adjusting the content of a single main element to improve the hardness and quench sensitivity of 7xxx Al alloys is difficult.

ZHOU et al [5] compared the hardness and quench sensitivity of the 7056 and 7055 alloys and found that the 7056 alloy with higher Zn and lower Cu contents exhibited similar surface layer hardness but much lower quench sensitivity than the 7055 alloy. Thus, decreasing Cu and increasing Zn contents may simultaneously increase the hardness and decrease quench sensitivity of 7xxx Al alloys, and further promote the application of ultra-thick Al alloys.

The effects of trace elements on mechanical

**Corresponding author:** Chong-yu LIU; Tel/Fax: +86-773-5896672; E-mail: lcy261@glut.edu.cn
DOI: 10.1016/S1003-6326(20)65476-0
1003-6326/© 2021 The Nonferrous Metals Society of China. Published by Elsevier B.V. & Science Press

properties and quench sensitivity of 7xxx Al alloys have been studied [10−13]. Zr addition can increase surface layer hardness, but it increases the quench sensitivity of 7xxx Al alloys [10,11]. Meanwhile, Ge addition can decrease quench sensitivity but decrease the strength of 7xxx Al alloys [12,13].

Sc is another important trace element in the new-type Al alloys. The addition of Sc into Al alloys can result in the formation of $Al_3(Sc,Zr)$ phases, which can refine their grains. Grain refinement caused by Sc addition can improve the mechanical properties [14−17], fatigue [18], superplasticity [19], corrosion resistance [20,21], and weldability [22,23] of 7xxx Al alloys. In recent years, Sc addition has been found to be able to affect the phase transformation process of 7xxx Al alloys [16,24]. For example, Sc addition could promote the precipitation of the $\eta'$ phase, but could also prevent the transformation of $\eta'$ phase to $\eta$ phase [16], and Sc addition could promote the formation of the $W$ phase in high-Cu-content 7xxx Al alloy [24]. The grain size and composition of the phases significantly influence the hardness of Al alloys, thereby influencing the quench sensitivity. However, studies about the effect of Sc addition on the quench sensitivity of 7xxx Al alloys are lacking.

In this study, the Zn, Cu, and Sc contents of 7xxx Al alloys were adjusted according to the chemical composition of a 7085 Al alloy. The effects of Zn and Cu contents and Sc addition on the phase composition, grain structure, hardness, and quench sensitivity of 7xxx Al alloys with high Zn contents were studied.

## 2 Experimental

7xxx Al alloys with four chemical compositions were fabricated by melting and casting. The compositions of the resulting four ingots are shown in Table 1. The ingots were subjected to homogenization treatment at 470 °C for 24 h and then hot-rolled to 30 mm. Four round rods were machined along the rolling direction, and the length and diameter of each rod were 125 and 25 mm, respectively.

The round rods were heated at 470 °C for 1 h and then quenched with Jominy end quench test equipment. Figure 1(a) shows the schematic diagram of the Jominy end quench test. The temperature change of the rod specimens at the positions with distances of 3, 30, 60, 90, and 120 mm from the quenching end was collected using a temperature thermocouple (Fig. 1(b)). Then, the cooling rates of the specimens were calculated. The peak aging hardness (T6) states of all the quenched alloys were obtained through artificial aging treatment at 120 °C for 24 h.

**Table 1** Chemical compositions of experimental alloys (wt.%)

| Sample | Zn | Mg | Cu | Zr | Fe | Sc | Al |
|---|---|---|---|---|---|---|---|
| 7085 | 7.59 | 1.69 | 1.64 | 0.11 | 0.11 | − | Bal. |
| High Zn–high Cu | 9.14 | 1.52 | 2.11 | 0.15 | 0.11 | − | Bal. |
| High Zn–low Cu | 9.68 | 1.55 | 1.28 | 0.12 | 0.10 | − | Bal. |
| Sc-added | 8.21 | 1.70 | 1.66 | 0.16 | 0.12 | 0.21 | Bal. |

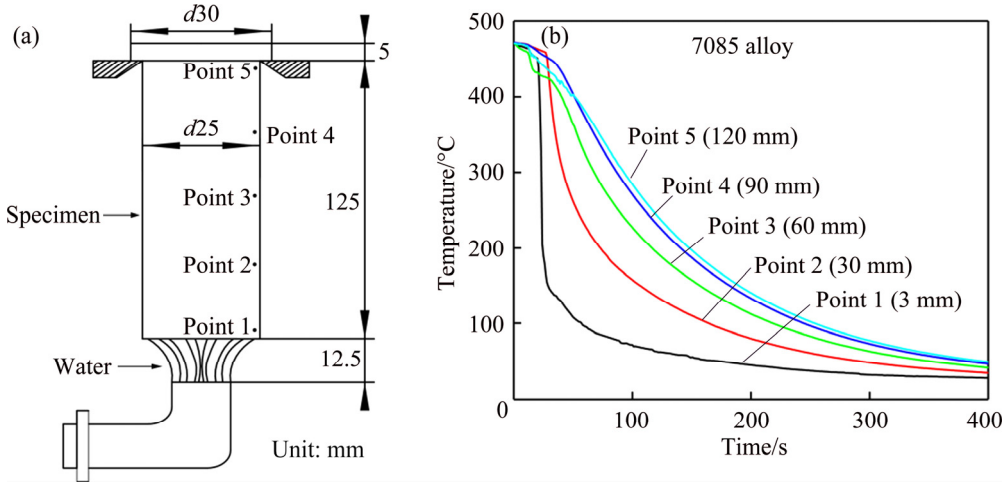


**Fig. 1** Schematic diagram of Jominy end quench test (a) and temperature change in test rod (7085 alloy) at different positions (b)

A microhardness tester was used to measure the Vickers hardness of the T6 alloys, and the hardness retention values of the samples at different positions were calculated. Optical microscope (OM, Leica-DMi8), scanning election microscope (SEM, Hitachi-S4800 and Zeiss Gemini−300), and transmission electron microscope (TEM, FEI-Tecnai $G^2$ F20 S-TWIN) were used to observe the microstructures of T6 alloys at different positions. Energy-dispersive X-ray spectroscope (EDS) on SEM and TEM was used to analyze the phase compositions of the T6 alloys. The OM and SEM specimens were polished using a polishing machine, and the OM images were obtained after etching with Keller reagent (1 mL HF + 1.5 mL HCl + 2.5 mL $HNO_3$ + 95 mL $H_2O$). The TEM specimens were prepared by mechanical grinding to a thickness of 0.1 mm, followed by thinning using a twin-jet electropolishing unit in a solution of 20 vol.% $HNO_3$ and 80 vol.% $CH_3OH$ at −20 °C. The voltages of the SEM and TEM tests were 15 and 200 kV, respectively.

## 3 Results

### 3.1 Cooling rate curve

Figure 2 shows the cooling rates at different positions of the alloy rods. The cooling rates of the rods decreased with increasing distance from the quenching end and Zn contents, and the addition of Sc slightly decreased the cooling rate of the 7085 alloy at the positions far from the quenching end.

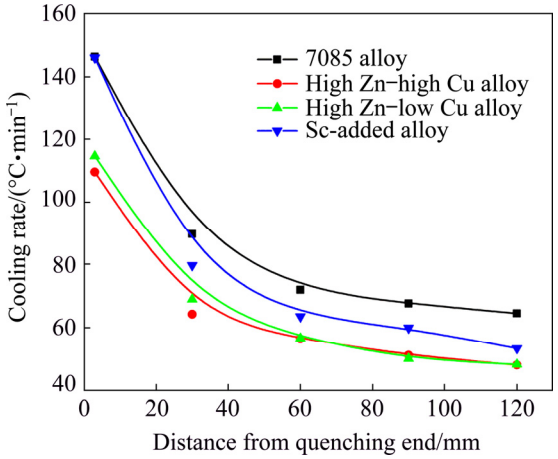


**Fig. 2** Cooling rates at different positions of alloy rods

### 3.2 Hardness curves

Figure 3(a) shows the hardness distribution of the T6 alloys. The high Zn−low Cu, high Zn−high Cu, and Sc-added alloys exhibited higher hardness than the 7085 alloy at the 3 mm position away from the quenching end (simply 3 mm position). In all the samples, the hardness decreased with increasing distance from the quenching end. The hardness of the high Zn−low Cu alloy at the position 120 mm away from the quenching end (120 mm position) was HV 173, which was higher than the values of the other alloys at the same position.

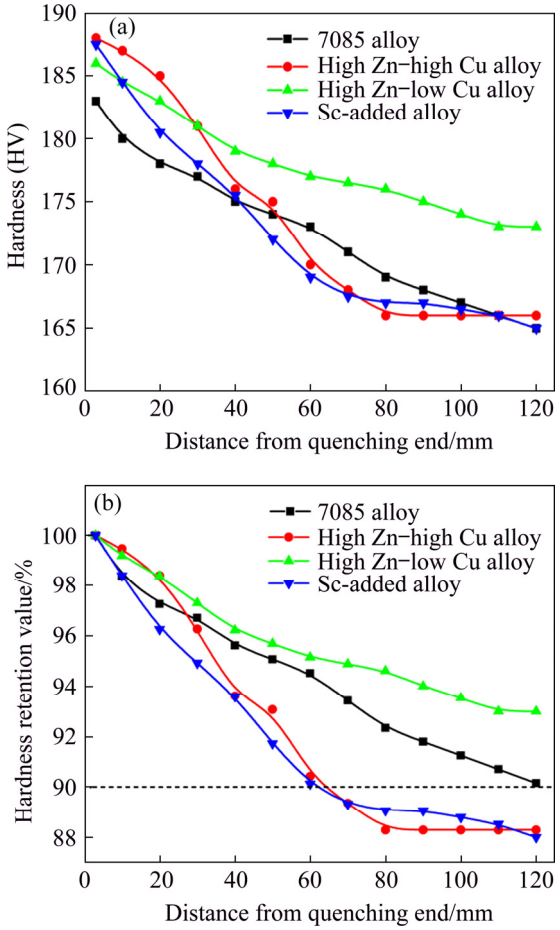


**Fig. 3** Hardness distribution of alloys along length direction (a) and hardness retention values of alloys at different positions (b)

Figure 3(b) shows the hardness retention values of the T6 alloys at different positions. The depths of the quenching layer referred to the distance from quenching end to the positions with 90% hardness retention values, and the large quenching layer depth corresponds to low quench sensitivity. The quenching layer depth of the 7085 Al alloy was 120 mm, and that of the high Zn−high Cu and Sc-added alloys was 60 mm. The hardness retention value of the high Zn−high Cu and Sc-added alloys at the 120 mm position was 88%.

The high Zn–low Cu alloy exhibited the lowest quench sensitivity, with a quenching layer depth that was greater than 120 mm and a hardness retention value as high as 93% at the 120 mm position.

### 3.3 Microstructures

Figure 4 shows the OM images of the alloys at the 3 and 120 mm positions. The grain size and morphology of the 7085 alloy at the 3 mm position were similar to those of the 7085 alloy at the 120 mm position, and the average grain size and grain morphology of the 7085 alloy were 200 μm and equiaxed shape, respectively (Figs. 4(a) and (b)). The high Zn–high Cu and high Zn–low Cu alloys exhibited the same grain structure characteristics as the 7085 alloy; their OM images are not displayed in this work. The 3 and 120 mm positions of the Sc-added alloy exhibited similar grain structure characteristics and contained elongated grains. The grain size of the Sc-added alloy was finer than that of the 7085 alloy, and the average short and long dimension sizes of the grains in the Sc-added alloy were 30 and 220 μm, respectively (Figs. 4(c) and (d)). Furthermore, the high density of sub-grain boundaries (SGBs) was also observed in the Sc-added alloy (Fig. 4(e)).

Figure 5 shows the SEM images of the 7085, high Zn−high Cu, and Sc-added alloys at the 3 mm position. The alloys had 5−20 μm coarse second phases with high densities (Figs. 5(a), (c), and (d)). The EDS results, which are not displayed in this work, showed that the coarse phases with irregular shapes in the alloys were $Al_7Cu_2Fe$ phases, and the

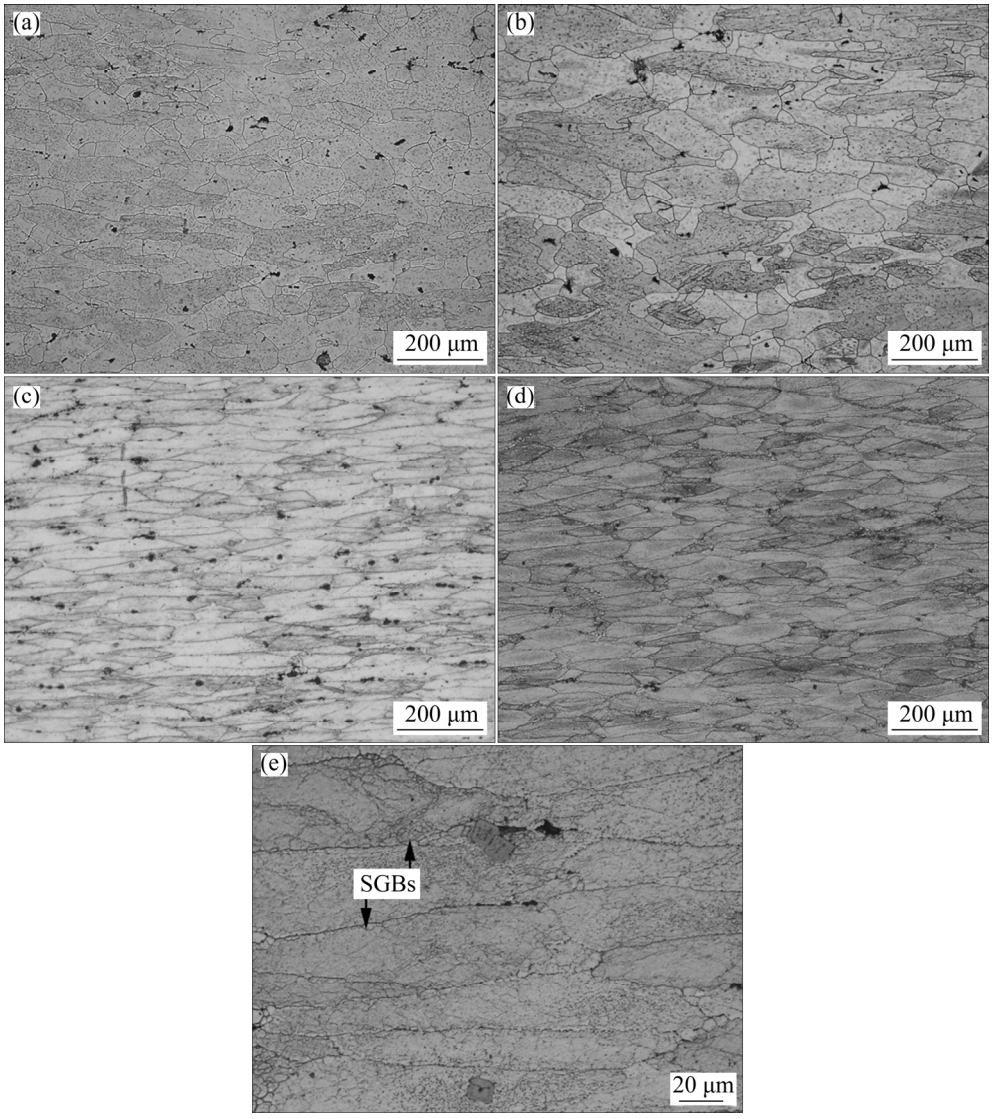


**Fig. 4** OM images of 7085 alloy at 3 mm (a) and 120 mm (b) positions and Sc-added alloy at 3 mm (c) and 120 mm (d, e) positions

rhombus phases in the Sc-added alloy were primary $Al_3(Sc,Zr)$ phases. The $Al_3Fe$ phase with 4 at.% Cu can be observed in the interior of the $Al_7Cu_2Fe$ phases (Fig. 5(b)). The high Zn–low Cu alloy at the 3 mm position exhibited the same coarse second phase structure characteristics as the 7085 and high Zn–high Cu alloys at the same position. The SEM images are not displayed here.

Figure 6 shows the SEM images of the alloys at the 120 mm position. The $Al_7Cu_2Fe$ phases were observed in all the alloys, and the phases that were lighter than the $Al_7Cu_2Fe$ phases were observed in the SEM images of 7085, high Zn−high Cu, and high Zn−low Cu alloys at the 120 mm position

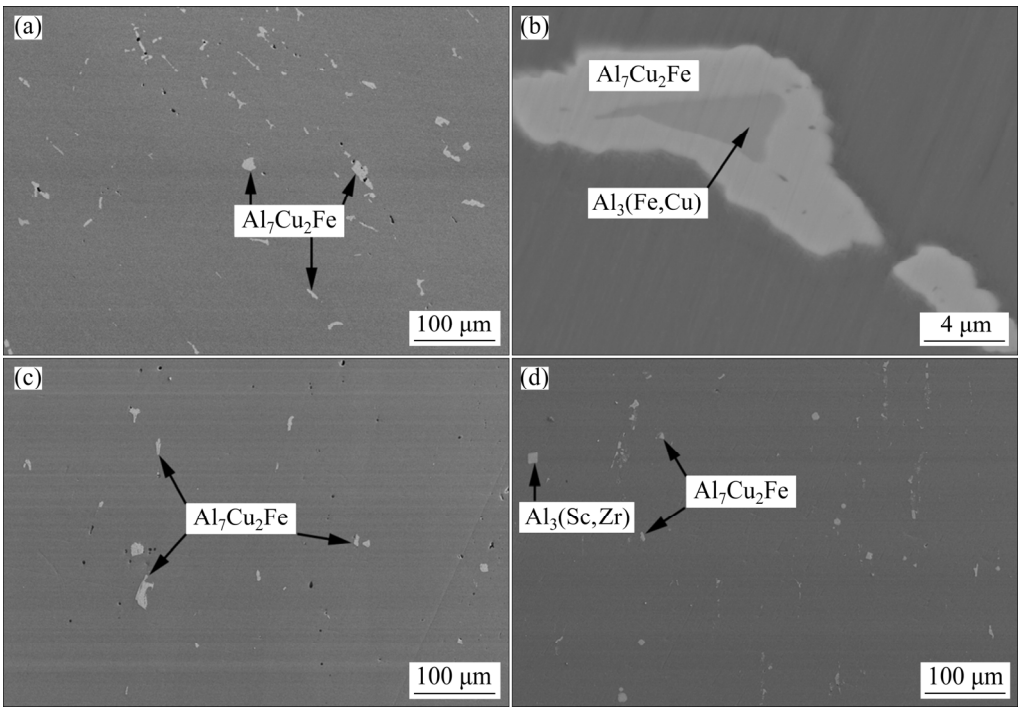


**Fig. 5** SEM images of 7085 (a, b), high Zn–high Cu (c), and Sc-added (d) alloys at 3 mm position

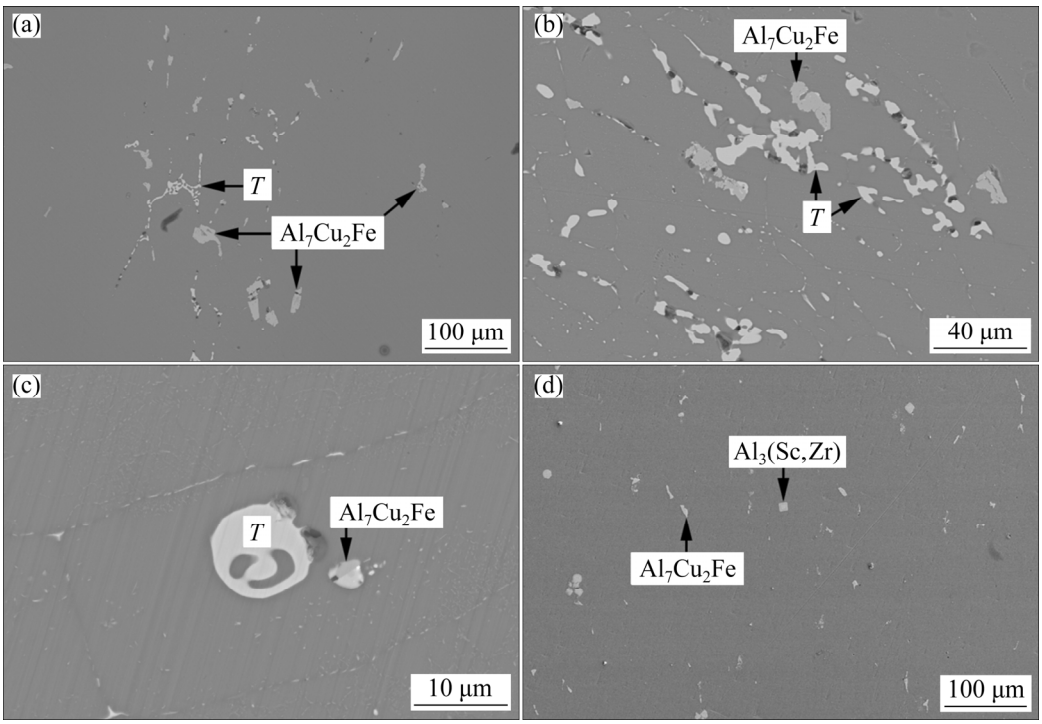


**Fig. 6** SEM images of 7085 (a), high Zn−high Cu (b), high Zn−low Cu (c), and Sc-added (d) alloys at 120 mm position

(Figs. 6(a)−(c)). The EDS results showed that the phases were *T*(AlZnMgCu) phases. The sizes of the *T* phases ranged from 5 to 20 μm. The *T* phases were not observed in the Sc-added alloy at the 120 mm position (Fig. 6(d)).

Figure 7 shows the TEM images of the alloys at the 3 mm position. Grain boundary precipitates (GBPs) with continuous distribution were observed at the GBs, and a high density of phases with sizes of several nanometers was obtained in the grain interiors of all the alloys (Figs. 7(a)−(e)). Compared with the 7085 alloy, the high Zn−high Cu alloy exhibited a high density of nanosized phases, and the high-resolution TEM image showed that these phases were $\eta'$ phases. The $Al_3Zr$ phase with a size of 30 nm could be observed in the 7085 and high

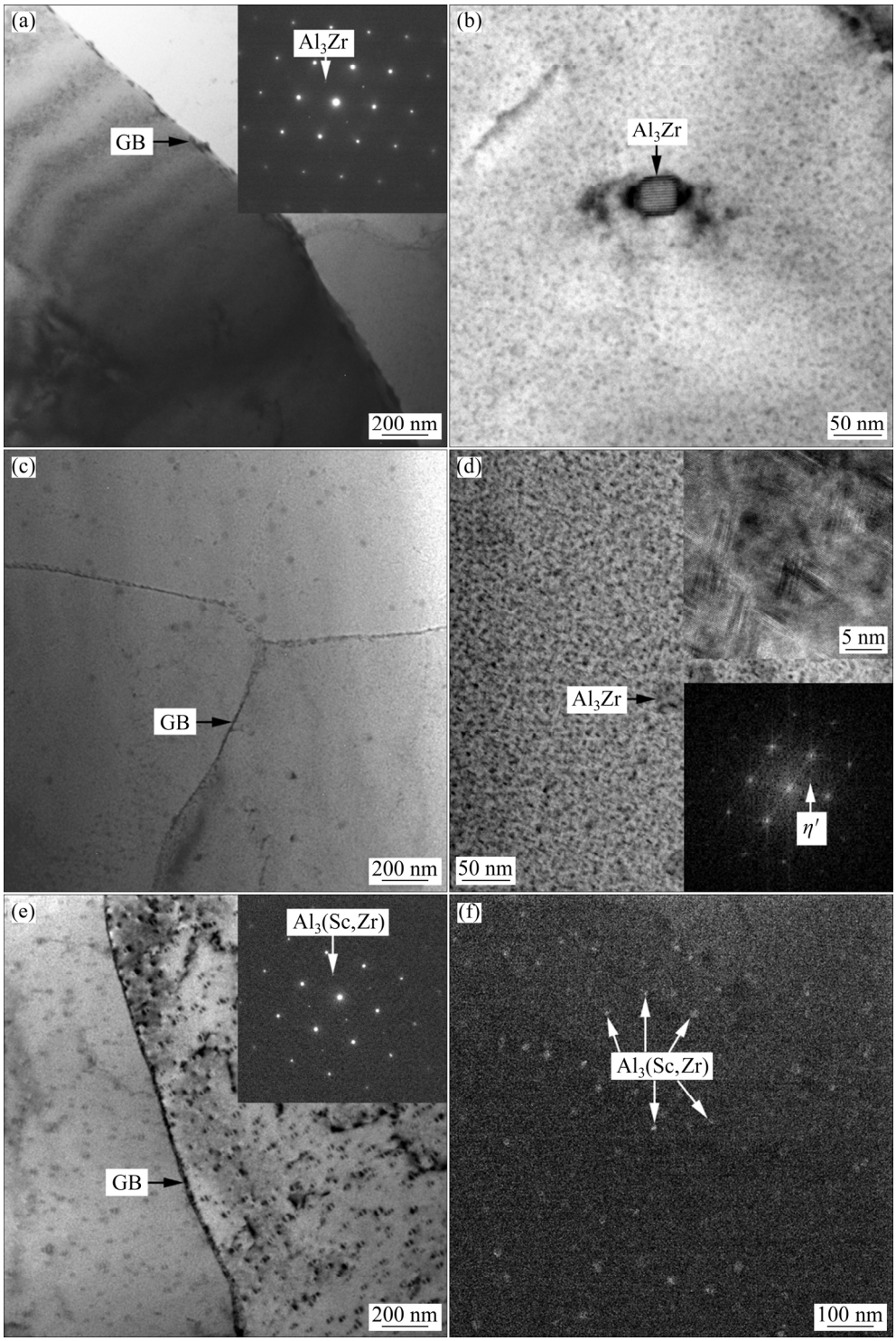


**Fig. 7** TEM images of 7085 (a, b), high Zn−high Cu (c, d), and Sc-added (e, f) alloys at 3 mm position

Zn−high Cu alloys (Figs. 7(b) and (d)). The structure characteristics of the precipitated phases of the high Zn−low Cu alloy at the 3 mm position were similar to those of the high Zn−high Cu alloy at the same position. The TEM images are not displayed in this work. A high density of $Al_3(Sc,Zr)$ phases was observed in the Sc-added alloy, and some of the $Al_3(Sc,Zr)$ phases were present at the GBs (Fig. 7(e)). The dark-field TEM image showed that the sizes of the $Al_3(Sc,Zr)$ phases were approximately 13 nm (Fig. 7(f)).

Figure 8 shows the TEM images of the 7085 and two high−Zn alloys at the 120 mm position. The GBPs that were several hundred nanometers in size could be observed at the GBs of all the alloys. The EDS results showed that the GBPs were

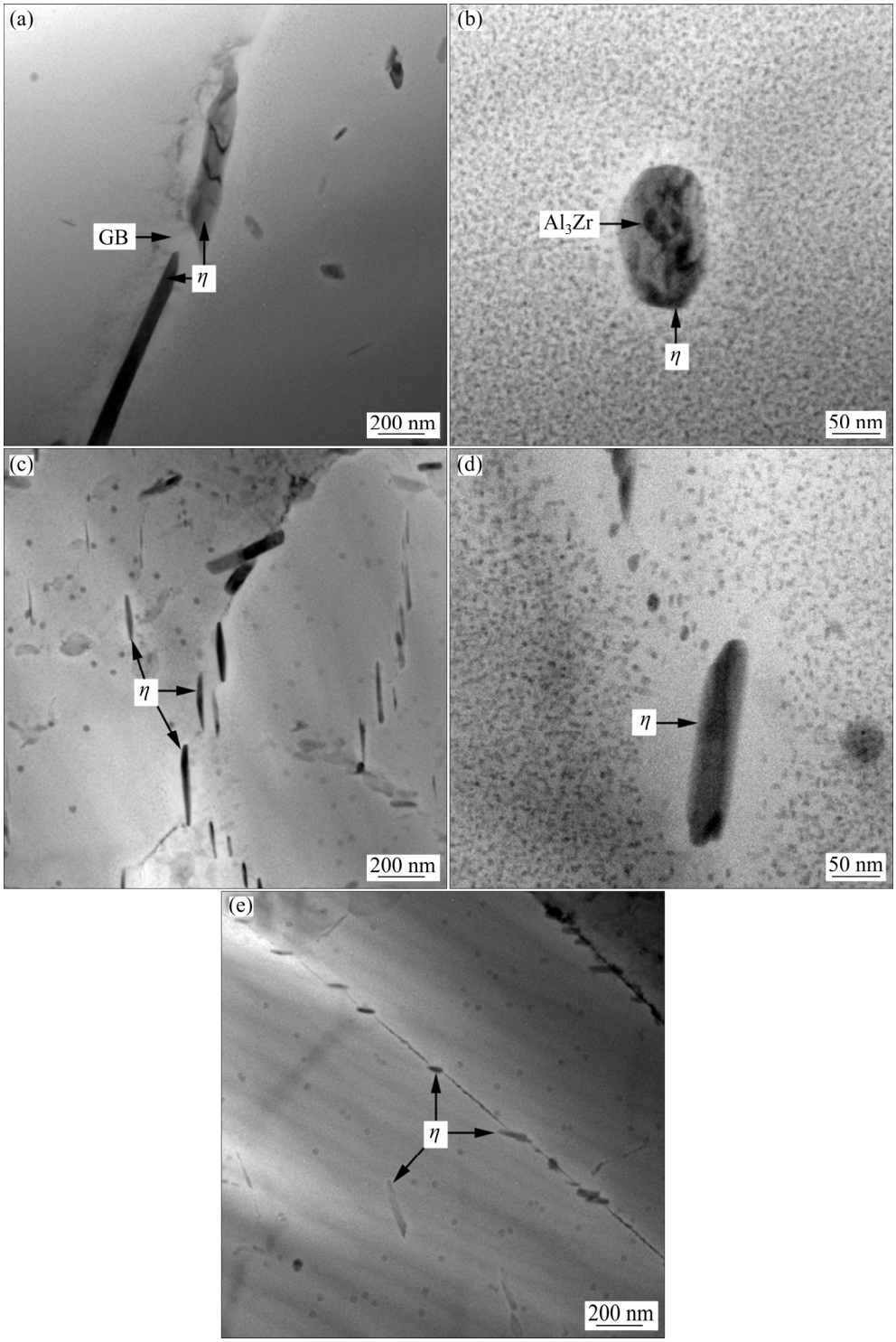


**Fig. 8** TEM images of 7085 (a, b), high Zn−high Cu (c, d), and high Zn−low Cu (e) alloys at 120 mm position

$\eta$($MgZn_2$) phases, and Cu was found in these phases. The $\eta$ phases were observed in the grain interiors of the alloys, and the two high-Zn alloys exhibited larger intragranular $\eta$ phases than the 7085 alloy (Figs. 8(a), (c), and (e)). The intragranular $\eta$ phases led to the formation of precipitate-free zones, as shown in Fig. 8(d), and the $Al_3Zr$ phases were observed in the $\eta$ phases (Fig. 8(b)).

Figure 9 shows the TEM images of Sc-added alloy at the 120 mm position. The $\eta$ phases were also observed at the GBs in the Sc-added alloy at the 120 mm position, and this alloy exhibited a high density of $\eta$ phases due to its fine grains and subgrains (Fig. 9(a)). The $Al_3$(Sc,Zr) phase was also observed in the $\eta$ phases, as shown in the high-angle annular dark-field imaging (HAADF) image (Fig. 9(b)). The *Y* (AlCuZn) phases, which were identified from a high-resolution TEM image, were obtained in the Sc-added alloy at the 120 mm position (Figs. 9(c) and (d)).

## 4 Discussion

The distance from the quenching end and chemical composition affected the cooling rate of the alloys. High Zn solution atom content decreased heat transfer rate in the Al alloys and then decreased the cooling rate during quenching. The GBs and phase affected the heat transfer rate in the alloys, and the Sc-added alloys with fine grains, high GB density and high density of nanosized $Al_3$(Sc,Zr) phases exhibited lower cooling rates than the 7085 alloy at the positions far from the quenching end. However, the effects of chemical composition and microstructure on the cooling rate of the 7xxx alloys were much smaller than those of the distance from the quenching end.

The grain structures of the 7xxx alloys in this study were not affected by Zn and Cu contents and cooling rate during quenching (Fig. 4). Sc addition

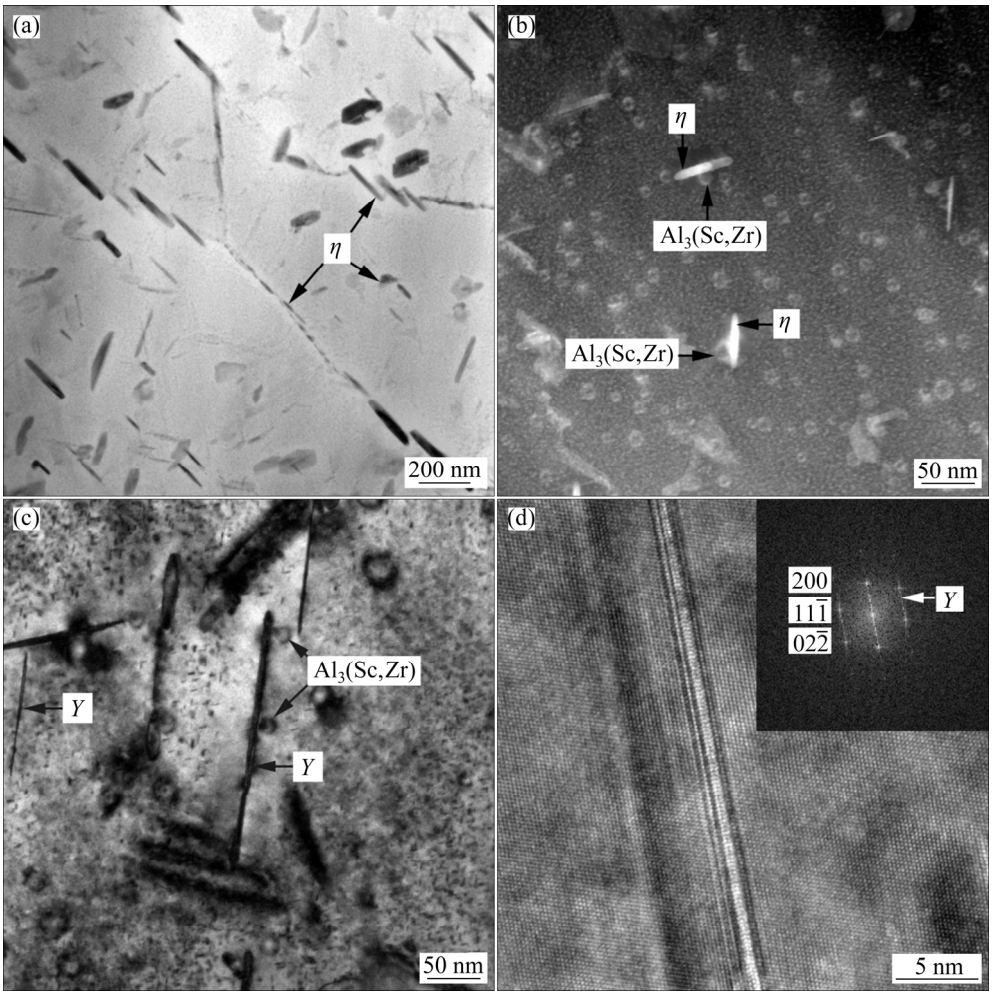


**Fig. 9** Low magnification (a), HAADF (b), high magnification (c), and high resolution (d) TEM images of Sc-added alloy at 120 mm position

led to the formation of primary $Al_3(Sc,Zr)$ phases (Fig. 5(d)), thereby promoting the heterogeneity and grain refinement of the 7xxx Al alloys during casting. The nanosized $Al_3(Sc,Zr)$ phases were precipitated during homogenization treatment, several of which were located at the GBs (Fig. 7(e)). The grain coarsening of the rolled 7xxx alloys during solid solution treatment can be effectively inhibited by $Al_3(Sc,Zr)$ precipitated phases [14−22,24]. Thus, the deformed grains can be retained in the Sc-added alloy after T6 treatment, and this alloy exhibited finer grains than other alloys (Fig. 4). The fine sub-grains, which formed during deformation before quenching, were also retained in the Sc-added alloy due to the pinning effect of $Al_3(Sc,Zr)$ precipitated phases. Thus, compared with Sc-free alloys, the Sc-added alloy exhibited a much higher density of SGBs (Fig. 4(e)).

The Fe contents of all the studied alloys were approximately 0.10 wt.%, and the low solubility of Fe in the Al lattice led to the Fe-containing phases being insoluble phases in the Al alloys. Thus, the sizes and densities of the $Al_7Cu_2Fe$ phases were not affected by the cooling rate (Figs. 5 and 6). The $Al_3(Fe,Cu)$ phase with low Cu content was observed in the cores of various $Al_7Cu_2Fe$ phases (Fig. 5(b)), indicating that the $Al_7Cu_2Fe$ phases were formed after the formation of the $Al_3(Fe,Cu)$ phases and may have evolved from the $Al_3(Fe,Cu)$ phase during heat treatment at high temperatures.

The $Al_3Zr$ precipitated phases in the 7xxx alloys were formed during homogenization treatment, and the $Al_3Zr$ precipitated phases were replaced by the $Al_3(Sc,Zr)$ phases in the Al alloys with Sc addition. The $Al_3Zr$ and $Al_3(Sc,Zr)$ phases exhibited high thermal stability during subsequent hot deformation or heat treatment. Thus, the sizes and densities of the $Al_3Zr$ and $Al_3(Sc,Zr)$ precipitated phases in the studied alloys were not affected by cooling rate during quenching (Figs. 7(b), 7(f), 8(b), 9(b), and 9(c)).

The high cooling rate of the alloy rods at the 3 mm position led to the formation of a supersaturated solid solution after quenching, and the subsequent aging treatment led to the precipitation of the $\eta'$ phases at this position. The large number of solid solution atoms in the high Zn alloys led to the increase in the density of $\eta'$ phase, which was higher than that of the 7085 alloy at the 3 mm position (Figs. 7(b) and (d)). Aging led to GBP formation with continuous distribution due to the high energy at the GBs.

The $\eta$ phases were precipitated at the 120 mm position of the alloy rods, and crystal defects, such as GBs, $Al_3Zr$/Al, and $Al_3(Sc,Zr)$/Al interfaces, promoted the precipitation of the $\eta$ phases due to their high energy. Compared with the 7085 alloy, the Sc-added alloy exhibited higher densities of GBs and SGBs, and the density of the $Al_3(Sc,Zr)$ phase in the Sc-added alloy was much higher than that of the $Al_3Zr$ phase in the 7085 alloy. Thus, the Sc-added alloy exhibited a higher density of $\eta$ phases at the 120 mm position than the 7085 alloy at the same position (Figs. 8(a) and 9(a)). The high solution atom content in the two high-Zn-content alloys promoted the formation of intragranular $\eta$ phases that were larger than those in the 7085 alloy (Figs. 8(c) and (e)). Subsequent aging treatment led to the precipitation of the $\eta'$ phases in the alloys at the 120 mm position. However, the PFZs without $\eta'$ phases were formed around the $\eta$ phases because the Zn and Mg atoms were consumed by the $\eta$ phases (Fig. 8(d)).

The low cooling rate of the alloy rods at the 120 mm position led to the formation of large *T* phases in the 7085 and two high-Zn-content alloys (Fig. 6). The *T* phases contain 25 at.% Cu, Thus, the high Zn−low Cu alloy exhibited lower volume fraction of *T* phases than 7085 and high Zn–high Cu alloys due to its low Cu content. *T* phases also contain 25 at.% Mg and 25 at.% Zn. Thus, more Mg and Zn solution atoms were retained in the high Zn−low Cu alloy after quenching, and subsequent aging led to the high Zn−low Cu alloy that exhibited a higher density of $\eta'$ phases than the 7085 and high Zn−high Cu alloys.

*T* phases were not observed in the Sc-added alloy at the 120 mm position. However, the *Y* phases were observed in the Sc-added alloy at the 120 mm position (Figs. 9(c) and (d)).

ZHANG et al [25] and LIU et al [26] found that the *Y* phases precipitated in the 7xxx Al alloy during cooling at a slow rate. However, the cooling rate of the Sc-added alloy at the 120 mm position was higher than that of the two high-Zn-content alloys at the same position during quenching (Fig. 2). Compared with other alloys, the Sc-added alloy exhibited a higher density of SGBs, and these SGBs could promote the nucleation points for the *Y*

phases during cooling [26]. Thus, the high cooling rate could lead to the precipitation of the *Y* phases in the Sc-added alloy. Furthermore, the Cu atoms were consumed by the *Y* phases, and then the formation of *T* phases was inhibited.

A schematic illustration of the effect of Zn and Cu contents and Sc addition on the microstructure of 7085 alloy at the 120 mm position is shown in Fig. 10. Increasing the Zn and Cu contents led to the increase in the volume fractions of $\eta$ and *T* phases in the 7085 alloy. Meanwhile, Sc addition led to the occurrence of grain refinement, increased volume fraction of $\eta$, *Y* phase formation, and *T* phase disappearance in the 7085 alloy.

The increased Zn content can enhance the $\eta'$ phase density of the 7085 alloy at the 3 mm position. Meanwhile, Sc addition can reduce the grain size of the 7085 alloy at the 3 mm position. High precipitation strengthening or high GB strengthening caused the high-Zn and Sc-added alloys to exhibit higher hardness than the 7085 alloy at the 3 mm position.

The $Al_3(Fe, Cu)$ phases exerted a low-reinforcement effect on the Al alloys due to their large sizes, and the phases did not change with the variation in cooling rate. However, the volume fractions of the $\eta$ and *T* phases in the 7xxx alloys increased with the decrease in cooling rate during quenching. The $\eta$ and *T* phases consumed Zn and Mg atoms and then inhibited the precipitation of the $\eta'$ phases. Thus, in an alloy, hardness decreased with the increase in distance from the quenching end due to the decrease in the precipitation strengthening effect along the length direction of the alloy rods.

The high Zn−high Cu alloy contained higher volume fractions of $\eta$ and *T* phases than the 7085 alloy at the 120 mm position. The $\eta$ and *T* phases were almost unable to reinforce the Al alloys due to their large sizes. The extra $\eta$ and *T* phases consumed additional Zn and Mg atoms. Thus, the precipitation strengthening effect of the high Zn−high Cu alloy at the 120 mm position after aging may not be higher than that in the 7085 alloy

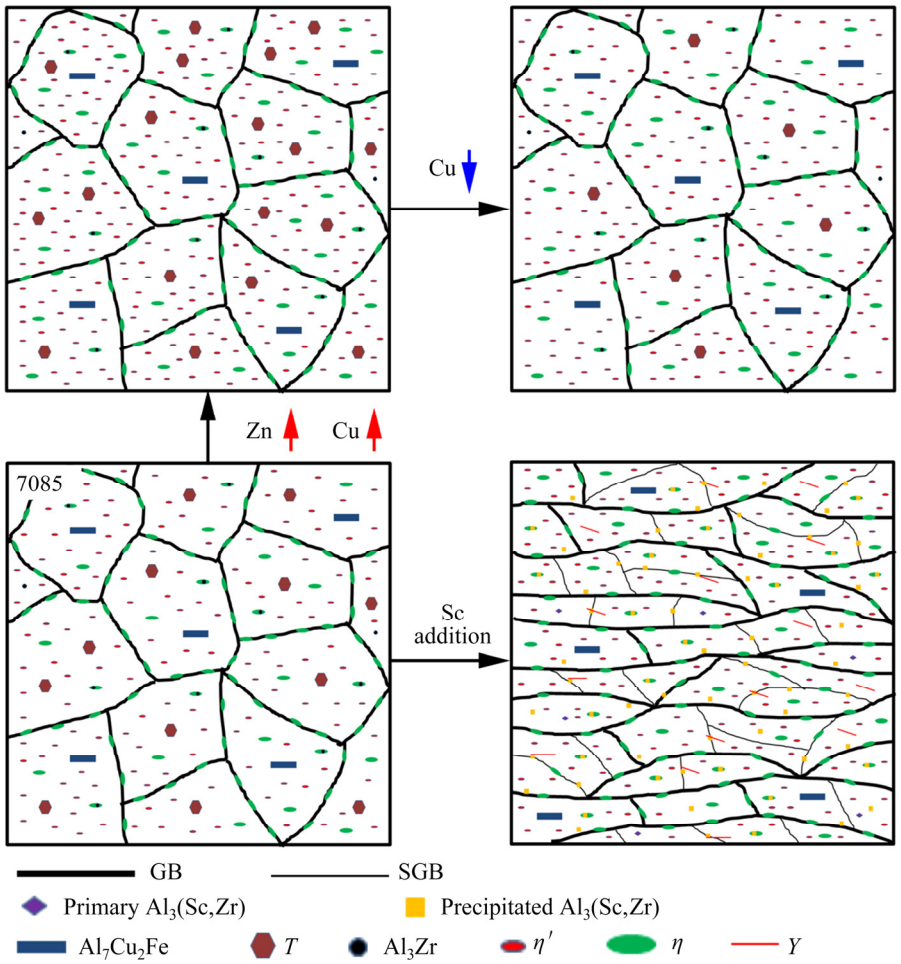


**Fig. 10** Schematic illustration of effect of Zn and Cu contents and Sc addition on microstructure of 7085 alloy at 120 mm position

at the same position, and the high Zn−high Cu and 7085 alloys exhibited the same hardness at the 120 mm position. The high hardness of the high Zn−high Cu alloy at the 3 mm position led to this alloy having lower hardness retention values at the 120 mm position and higher quench sensitivity than the 7085 alloy.

The *Y* phases with a high aspect ratio could provide a high precipitation strengthening effect to Al alloys [26]. However, the low volume fraction of *Y* phases in the Sc-added alloy at the 120 mm position limited the strengthening effect of *Y* phases. Compared with the 7085 alloy, the Sc-added alloy exhibited higher volume fraction of $\eta$ phase at the 120 mm position and low precipitation strengthening. The net effect of low precipitation strengthening and high GB strengthening caused the Sc-added alloy to exhibit the same hardness as the 7085 alloy at the 120 mm position, and the high hardness of Sc-added alloy at the 3 mm position also led to this alloy to have lower hardness retention values at the 120 mm position and higher quench sensitivity than the 7085 alloy.

Low Cu content in the high Zn−low Cu alloy decreased the volume fraction of the *T* phase at the 120 mm position, and additional Zn and Mg atoms were retained at this position after quenching. The higher hardness and hardness retention value of the high Zn−low Cu alloy compared with the other samples at the 120 mm position can be attributed to the high precipitation strengthening effect. Thus, the high Zn−low Cu alloy has the lowest quench sensitivity of all the studied alloys.

## 5 Conclusions

(1) The two high-Zn alloys exhibited higher $\eta'$ phase density at the 3 mm position than the 7085 alloy at the same position. For the 120 mm position, the high Zn−low Cu alloy exhibited lower volume fractions of $\eta$ and *T* phases than the high Zn−high Cu alloy, and these two phases consumed high amounts of Mg and Zn solution atoms, thereby reducing the densities of the $\eta'$ phases in the alloys after aging.

(2) Sc addition led to the formation of $Al_3$(Sc,Zr) phases, which refined the grains and inhibited recrystallization. The grain refinement could enhance the density of the $\eta$ phases and the high density of SGBs could promote the formation of *Y* phases in the Sc-added alloy at the 120 mm position.

(3) Two high-Zn alloys and a Sc-added alloy exhibited higher hardness than the 7085 alloy at the 3 mm position due to their higher precipitation and GB strengthening effect, respectively. The high Zn−low Cu alloy exhibited the lowest quench sensitivity, and its hardness retention value at the 120 mm position reached as high as 93%. The high Zn−high Cu and Sc-added alloys exhibited higher quench sensitivity than the 7085 alloy, although the three alloys exhibited a similar hardness at the 120 mm position.

## Acknowledgments

The authors are grateful for the financial supports from the Science and Technology Major Project of Guangxi, China (GKAA17202007).

## References

[1] ZHENG Y L, LI C B, LIU S D, DENG Y L, ZHANG X M. Effect of homogenization time on quench sensitivity of 7085 aluminum alloy [J]. Transactions of Nonferrous Metals Society of China, 2014, 24: 2275−2281.

[2] LI P Y, XIONG B Q, ZHANG Y A, LI Z H, ZHU B H, WANG F, LIU H W. Quench sensitivity and microstructure character of high strength AA7050 [J]. Transactions of Nonferrous Metals Society of China, 2012, 22: 268−274.

[3] FU P, ZHOU P, XIE Z W, WU H Y, CHEN J G. Experimental and CFD investigations on cooling process of end-quench test [J]. Transactions of Nonferrous Metals Society of China, 2019, 29: 2440−2446.

[4] LIM S T, YUN S J, NAM S W. Improved quench sensitivity in modified aluminum alloy 7175 for thick forging applications [J]. Materials Science and Engineering A, 2004, 371: 82−90.

[5] ZHOU L, CHEN K H, CHEN S Y, ZHANG X L, FAN S M, HUANG L P. Comparison of hardenability and over-aging precipitation behaviour of three 7xxx aluminium alloys [J]. Materials Science and Technology, 2019, 35: 637−644.

[6] ZHANG Z H, XIONG B Q, LIU S F, ZHU B H, ZUO Y T. Changes of microstructure of different quench sensitivity 7000 aluminum alloy after end quenching [J]. Rare Metals, 2014, 33: 270−275.

[7] NIE B H, LIU P Y, ZHOU T T. Effect of compositions on the quenching sensitivity of 7050 and 7085 alloys [J]. Materials Science and Engineering A, 2016, 667: 106−114.

[8] DENG Y L, WAN L, ZHANG Y Y, ZHANG X M. Influence of Mg content on quench sensitivity of Al−Zn−Mg−Cu aluminum alloys [J]. Journal of Alloys and Compounds, 2011, 509: 4636−4642.

[9] PENG Y H, LIU C Y, MA Z Y, JIANG H J, HUANG H F. Hardness, quench sensitivity, and electrical conductivity of 7xxx Al alloys with high Zn concentrations [J]. Science China (Technological Sciences), 2020, 63: 953−959.

[10] LIU S D, ZHANG X M, CHEN M A, YOU J H, ZHANG X Y. Effect of Zr content on quench sensitivity of AlZnMgCu alloys [J]. Transactions of Nonferrous Metals Society of China, 2007, 17: 787−792.
[11] LIU S D, LIU W J, ZHANG Y, ZHANG X M, DENG Y L. Effect of microstructure on the quench sensitivity of AlZnMgCu alloys [J]. Journal of Alloys and Compounds, 2010, 507: 53−61.
[12] LIN L H, LIU Z Y, BAI S, YING P Y, WANG X H. Effects of germanium on quench sensitivity in Al−Zn−Mg−Zr alloy [J]. Materials & Design, 2015, 86: 679−685.
[13] LIN L H, LIU Z Y, BAI S, ZHOU Y R, LIU W J, LV Q. Effects of Ge and Ag additions on quench sensitivity and mechanical properties of an Al−Zn−Mg−Cu alloy [J]. Materials Science and Engineering A, 2017, 682: 640−647.
[14] XIAO Q F, HUANG J W, JIANG Y G, JIANG F Q, WU Y F, XU G F. Effects of minor Sc and Zr additions on mechanical properties and microstructure evolution of Al−Zn−Mg−Cu alloys [J]. Transactions of Nonferrous Metals Society of China, 2020, 30: 1429−1438.
[15] CHARIT I, MISHRA R S. Effect of friction stir processed microstructure on tensile properties of an Al−Zn−Mg−Sc alloy upon subsequent aging heat treatment [J]. Journal of Materials Science & Technology, 2018, 34: 214−218.
[16] TENG G B, LIU C Y, MA Z Y, ZHOU W B, WEI L L, CHEN Y, LI J, MO Y F. Effects of minor Sc addition on the microstructure and mechanical properties of 7055 Al alloy during aging [J]. Materials Science and Engineering A, 2018, 713: 61−66.
[17] SPIERINGS A B, DAWSON K, UGGOWITZER P J, WEGENER K. Influence of SLM scan-speed on microstructure, precipitation of $Al_3Sc$ particles and mechanical properties in Sc- and Zr-modified Al−Mg alloys [J]. Materials & Design, 2018, 140: 134−143.
[18] HYUN C Y, KIM H K. Fatigue properties of a modified 7075 aluminum alloy containing scandium [J]. Journal of Materials Science, 2010, 45: 3067−3072.
[19] CHARIT I, MISHRA R S. Low temperature superplasticity in a friction-stir-processed ultrafine grained Al−Zn−Mg−Sc alloy [J]. Acta Materialia, 2005, 53: 4211−4223.
[20] LI B, PAN Q L, CHEN C P, YIN Z M. Effect of aging time on precipitation behavior, mechanical and corrosion properties of a novel Al−Zn−Mg−Sc−Zr alloy [J]. Transactions of Nonferrous Metals Society of China, 2016, 26: 2263−2275.
[21] LI Z M, JIANG H C, WANG Y L, ZHANG D, YAN D S, RONG L J. Effect of minor Sc addition on microstructure and stress corrosion cracking behavior of medium strength Al−Zn−Mg alloy [J]. Journal of Materials Science & Technology, 2018, 34: 1172−1179.
[22] DENG Y, PENG B, XU G F, PAN Q L, YIN Z M, YE R, WANG Y J, LU L Y. Effects of Sc and Zr on mechanical property and microstructure of tungsten inert gas and friction stir welded aerospace high strength Al−Zn−Mg alloys [J]. Materials Science and Engineering A, 2015, 639: 500−513.
[23] GAO Q W, SHU F Y, HE P, DU W B. Microstructure and impact mechanical properties of multi-layer and multi-pass TIG welded joints of Al−Zn−Mg alloy plates [J]. Transactions of Nonferrous Metals Society of China, 2019, 29: 2496−2505.
[24] LIU C Y, TENG G B, MA Z Y, WEI L L, ZHANG B, CHEN Y. Effects of Sc and Zr microalloying on the microstructure and mechanical properties of high Cu content 7xxx Al alloy [J]. International Journal of Minerals Metallurgy and Materials, 2019, 26: 1559−1569.
[25] ZHANG Y, WEYLAND M, MILKEREIT B, REICH M, ROMETSCH P A. Precipitation of a new platelet phase during the quenching of an Al−Zn−Mg−Cu alloy [J]. Scientific Reports, 2016, 6: 1−9.
[26] LIU S D, LI Q, LIN H Q, SUN L, LONG T, YE L Y, DENG Y L. Effect of quench-induced precipitation on microstructure and mechanical properties of 7085 aluminum alloy [J]. Materials & Design, 2017, 132: 119−128.

# Cu 含量和 Sc 添加对高锌 Al−Zn−Mg−Cu 合金淬火敏感性和显微组织的影响

彭英浩，刘崇宇，韦莉莉，江鸿杰，戈震江

桂林理工大学 有色金属及材料加工新技术教育部重点实验室，桂林 541004

**摘　要：**根据 7085 合金成分，调整 7xxx 铝合金中 Zn、Cu 和 Sc 的含量；研究 Zn、Cu 含量及 Sc 添加对 7xxx 铝合金显微组织、硬度和淬火敏感性的影响。在距淬火端 3 mm 处，高 Zn 和 Sc 添加合金的硬度值高于 7085 合金的。在距淬火端 120 mm 处，$\eta$ 和 $T$ 相的密度随 Zn 和 Cu 含量的增加而增加，Sc 添加导致形成 $Y$ 相和更多的 $\eta$ 相。与 7085 合金相比，高 Zn 高 Cu 和 Sc 添加合金具有更高的淬火敏感性。增加 Zn 含量并降低 Cu 含量可在提高 7085 合金硬度的同时降低其淬火敏感性。

**关键词：**Al−Zn−Mg−Cu 合金；淬火敏感性；$Al_3(Sc, Zr)$；$Y$ 相；晶界

**(Edited by Wei-ping CHEN)**